Probabilistic reliability analysis of carbon-carbon composite nozzle exit cone with uncertain parameters

Weihua Xie [*], Yuanjian Yang [†] and Songhe. Meng [*],

Science and Technology on Advanced Composites in Special Environment Laboratory, Harbin Institute of Technology, Harbin, China, 150080

Tao Peng [‡]

STAR UAV Systems co., Ltd., Chengdu, China, 610200

Jie Yuan [※]

Imperial College London, UK, SW7 2AZ

Fabrizio Scarpa [§]

University of Bristol, Bristol, UK, BS8 1TR

Chenghai Xu [☆], and Hua Jin [☆]

Science and Technology on Advanced Composites in Special Environment Laboratory, Harbin Institute of Technology, Harbin, China, 150080

ABSTRACT: We describe in this paper a methodology to perform the probabilistic and reliability-based design of a novel carbon/carbon rocket nozzle subjected to operational thermal and mechanical loads. In this methodology the nozzle is represented by a multiphysics finite element model capable of predicting the temperature and stress fields of the exit cone. The analysis shows

[*] Professor, Science and Technology on Advanced Composites in Special Environment Laboratory, Harbin Institute of Technology, No.2 Yikuang Street, Harbin 150080, China.

[†] Ph.D. Student, Science and Technology on Advanced Composites in Special Environment Laboratory, Harbin Institute of Technology, No.2 Yikuang Street, Harbin 150080, China.

[‡] Senior engineer, STAR UAV Systems co., Ltd. No.2999 Westport Avenue, Shuangliu District, Chengdu, China.

[※] Ph.D. Dynamics Group, Department of Mechanical Engineering, Imperial College London, SW7 2AZ, London, UK.

[§] Professor, Bristol Composites Institute (ACCIS), University of Bristol, BS8 1TR Bristol, UK.

[☆] Associate professor, Science and Technology on Advanced Composites in Special Environment Laboratory, Harbin Institute of Technology, No.2 Yikuang Street, Harbin 150080, China.

that the most likely failure modes of the exit cone are related to compressive loading along the axial and hoop directions, and interlaminar shear. The probabilistic models used in this methodology account for the uncertainty of the material properties by using uniform and normal distributions and different variances. The reliability analysis is performed by using surface response methods. A global sensitivity analysis is also carried out using polynomial expansion chaos surface response models. A particular novelty of analysis is the use of Sobol indices to rank the importance of the single uncertain parameters in the models. The methodology provides a high level of confidence and robustness in determining that the axial thermal conductivity of the carbon/carbon material is the most critical material property to affect the three main failure modes, while the coefficient of the thermal expansion and the heat capacity play a very marginal role.

Keywords: Rocket nozzle; Exit cone; Reliability; Carbon/carbon; Uncertainty

Nomenclature

M = performance function

R = the capability

S = the response

R_1 = the shear strength, MPa

S_{12} = the shear stress, MPa

R_2 = the axial compressive strength, MPa

S_{22} = the axial compressive stress, MPa

R_3 = the hoop compressive strength, MPa

S_{33} = the hoop compressive stress, MPa

$x1$ = thermal expansion coefficient, 1/K

$x2$ = heat capacity, J/K

$x3$ = radial thermal conductivity, W/(m·K)

x4 = axial thermal conductivity, W/(m·K)

x5 = axial elastic moduli, MPa

x6 = radial elastic moduli, MPa

x7 = density, kg/m^3

1 Introduction

Carbon/carbon (C/C) nozzles constitute one of the more advanced components of Solid Rocket Motor (SRM) technology developed in recent years. Compared with a nozzle made from conventional materials, the carbon/carbon version involves a simplified design that produces a reduction in weight and internal ablation, and also features improved operational reliability. The operational environment of a solid rocket nozzle is very complex and challenging, with temperatures usually exceeding 3000°C and the presence of high pressure fields. The internal part of the nozzle is also subjected to sharp heat flux gradients and erosion. The short time burn generates some significant temperature gradients, and the complex thermodynamic environment generated by the presence of high pressures presents a critical challenge to the structural design of the rocket nozzle. The C/C nozzle exit cone structure is one of the most critical components in the SRM system, leading to potential failures during use.

Several efforts have been devoted to understanding the behavior of C/C composites at high temperatures [1-5]. Li *et al* [1] and Peng *et al* [2] investigated the microstructure and the ablation mechanism of C/C composites with scanning electron microscopy. Other research groups have focused on the effect of the ablative environment on the ablation behavior of C/C composites and have obtained valuable performance data. For example, Liu *et al* [3] studied the ablation characteristics of a C/C composite in a lab-scale solid rocket motor under a flux of

combustion products containing a high content of particulate alumina. Zaman *et al* [4] reported on the residual mechanical and thermophysical properties of C/C composites repeatedly ablated using 3000 °C oxyacetylene flame. From the numerical standpoint, Vignoles et al., [5] identified an efficient method to simulate the ablation of C/C composites by considering the bulk transport of reactants and heterogeneous mass transfer conditions. In recent years, several groups have also started to consider the ablation behavior of ceramic based nozzles doped with ceramic composition (e.g. ZrB2, ZrC, etc.) for enhanced performance at high temperatures [6, 7]. These works have built on the know-how accumulated on studying traditional C/C nozzles

Other significant activities related to C/C nozzle design have considered various aspects of heat transfer [8-10]. The analysis of the reliability of C/C composite nozzle exit cone structures is however scarcely represented in open literature [11, 12]. The reasons behind this lack of information are mainly related to the significant costs involved in the development and testing of these composites, and also confidentiality issues related to intellectual property ownership [13]. The resources involved in obtaining large amounts of experimental data may be prohibitive, and that justifies the use of reliability-based models to design solid rocket motor components. The results from system reliability analyses calculated on small data samples are affected by significant errors. Therefore numerical models have been widely used to simulate the thermal-structural response of the nozzle and integrate the reliability-based approach [13-17]. Morozov and de la Beaujardiere [13] developed a finite element method to investigate the dynamic thermo-structural response of a composite rocket nozzle throat. Goyal *et al* [16] developed reliable reduced size models based on 2D plane strain assumptions for SRM structural analysis. Turchi *et al* [17] suggested a numerical approach to describe a carbon–

phenolic SRM nozzle model and then investigated the role of the most important uncertainty parameters affecting the design. Heller *et al* [11, 12] pioneered a methodology for reliability analysis of C/C composites, and analyzed the stress state of a cylindrical structure consisting of multiple layers of C/C composite under thermal and pressure shock by assuming elasticity within the structure. The reliability of the composite configuration was also calculated. Bozkaya *et al* [18, 19] and Akpan and Wong [20] developed some useful and efficient methods for the sensitivity analysis and reliability calculations [21] based on surface response methods (SRM) and Monte Carlo simulation techniques.

In this paper we describe a probabilistic design methodology to assess, at the initial design stage, the reliability of carbon/carbon rocket nozzles under thermal and mechanical load conditions. The proposed finite element methodology allows the estimation of the reliability and probability using a combination of surface response methods and sensitivity analysis based on Sobol's approach with Polynomial Chaos expansions for the surface responses. A particular advantage of this approach also consists in the reduction of the computational resources required to perform the overall analysis.

The paper is organized as follows. In the first section we introduce a numerical multi-physics (thermal and structural) finite element analysis methodology to design a C/C exit cone with uncertain parameters, and present a method to estimate the probability of structural failure by combining the finite element model with response surface methods. In the second part of the paper the reliability metrics of the exit cone are calculated. Finally, the extent and the influence of different failure modes on structural reliability are analyzed and discussed. The global

sensitivity of the uncertain parameters to the failure modes is also evaluated through a Sobol analysis.

2 Thermal stress and failure mode analysis of the C/C exit cone

2.1 Model of the rocket nozzle

The nozzle is represented as an axisymmetric structure (Figure 1). The nozzle consists of a throat insert, an exit cone, a back wall, the inlet section and a metal flange. The exit cone is made from 2D needle-punched felt reinforced C/C composites [22, 23]. Carbon-felt reinforced C/C composites constitute the throat, and carbon cloth phenolic makes its inlet. The back wall insulation is made of silica cloth phenolic insulation materials, and high-strength alloy steel is used for the metal flange. The exit cone and the throat insert are bonded together by an adhesive layer; the exit cone and the back wall are also bonded by a similar adhesive layer (Figure 1). A gap is present in the connecting section between the throat insert and the exit cone to release the thermal stress and avoid a deformation mismatch caused by the stress concentration at high temperatures. The silica cloth phenolic can isolate the hot and cooled substructures, and makes it possible for the metal flange to stay within its operational temperature range. The main role of the metal flange is to connect the composite nozzle to the motor casing, and fix the geometry of the exit cone. The properties of the materials used in the design are listed in Tables 1, 2 and 3. The parameters k, c, α, υ, E, ρ represent the thermal conductivities, heat capacities, thermal expansion coefficients, Poisson's ratios, elastic moduli and densities, respectively. The subscripts 1, 2 and 3 indicate the principal orthotropic directions of the materials (i.e., the radial, tangential and axial directions in a cylindrical coordinate system) respectively.

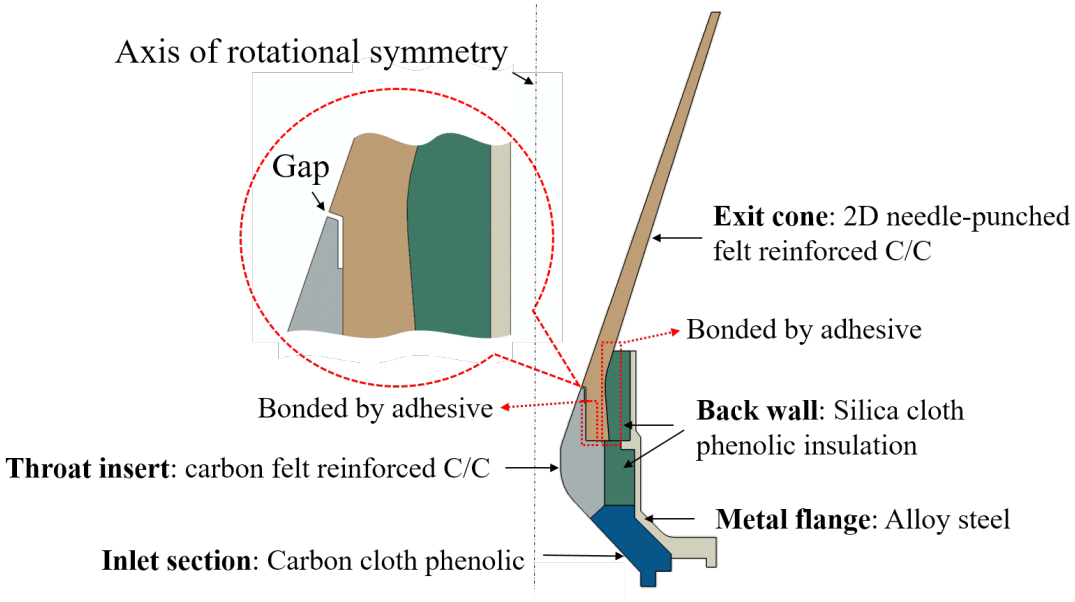

Fig. 1. Two-dimensional view of the nozzle structure

Table 1 Thermal properties of the 2D needle-punched felt reinforced C/C

Temperature [°C]	α [K^{-1}]	c [J/(kg·K)]	k [W/(m·K)]	
			k_{11}	k_{22} =k_{33}
20	1.15E-07	777.6	7.18	16.47
200	6.82E-07	1286.4	9.09	21.05
400	8.64E-07	1660.8	9.95	23.34
600	1.24E-06	1824.0	9.73	22.39
800	1.52E-06	1929.6	9.94	22.36
1000	1.76E-06	1996.8	10.29	22.20
1200	1.97E-06	2054.4	10.47	23.22
1400	2.17E-06	2121.6	10.65	23.70
1600	2.39E-06	2150.4	11.25	24.08
1800	2.70E-06	2208.0	11.66	25.01

Table 2 Mechanical properties of needle-punched felt reinforced C/C

Temperature, °C	E_{11} [GPa] (Out-plane)	E_{22}=E_{33} [GPa] (In-plane)	υ		Density [kg/m^3]
			υ_{12}= υ_{13}	υ_{23}	
20	7.90	29.50	0.1	0.24	1540
1200	/	33.84	/	/	/
1600	/	31.13	/	/	/

Table 3 Material properties of other materials other than needle-punched felt reinforced C/C

Materials / Properties		Silica cloth phenolic insulation 20°C	300°C	Carbon-felt reinforced C/C	Carbon cloth phenolic	Alloy steel
k [W/(m·K)]	k_{11}	0.61	0.82	80.4	0.84	27.63
	k_{22}	0.53	0.74	30.5		
	k_{33}	0.53	0.74	30.5		
c [J/(kg·K)]	c_{11}	1013	1705	1200	1189	473.1
	c_{22}	1072	1722			
	c_{33}	1072	1722			
α [$10^{-6}K^{-1}$]	α_{11}	12.40	1.01	3.37	8.2	12.92
	α_{22}	11.72	1.31	1.45		
	α_{33}	11.72	1.31	1.45		

υ	0.11	0.1	0.26	0.3
E [GPa]	14.5	13.2	11	196
ρ [kg/m^3]	1640	1820	1800	7750

The thermal domain (i.e., the transient heat transfer) representing the nozzle is modeled as axisymmetric because of the rotational symmetry of the nozzle geometry. The gas flow generates nearly 6MPa pressure [13] and wall shear stresses on the inner wall of the nozzle. Because the magnitude of the wall shear stress is very small [22], its influence on the nozzle performance can be therefore neglected. The pressure generated by the gas flow generates the main mechanical load. The heat transfers between the high-temperature gas and the inner wall generally can be classified into convective, radiant and conductive. The forced convective heat is the most significant factor for the heat transfer [23-26].

To simplify the model we impose the following assumptions: (1) only convective heat transfers between the flow and the nozzle are considered on the inner wall of the nozzle; radiation and conduction are ignored [23-26]. The mechanical erosion of the material and the ablation of the inner nozzle wall are also neglected [27, 28]. (2) Only convective heat transfer between the air and the outer wall of the nozzle is considered, and the radiation heat loss is neglected [29-32]. (3) The flow field parameters (pressure and temperature) do not change for a SRM in steady-state operations (4) The thermally induced erosion of the insulation material is ignored [27, 28].

The temperature profile around the nozzle, the gas pressure and the convective heat transfer coefficient vary with the axial distance (Fig. 2. (a) and (b)) [32].

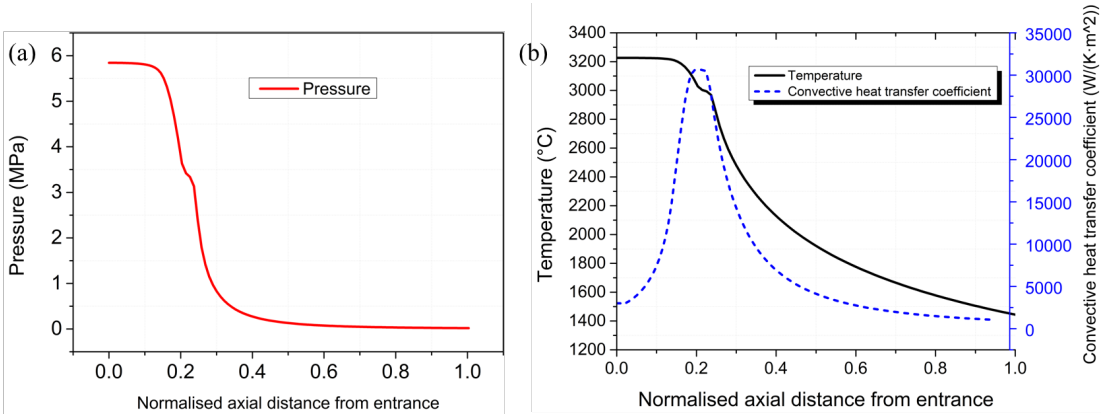

Fig. 2. Variations of the flow gas temperature, convective heat transfer coefficient (a) and gas pressure (b) with the axial position

The following boundary conditions and constraints are used in the numerical analysis of nozzle: (a) The heat transfer between the outer wall of the exit cone and the ambient air is represented by natural convection only, with a convective heat transfer coefficient of 5W/ (m^2·K) [27, 28]. (b) The body of the nozzle is initially at room temperature (20 °C), which is representative of ground test conditions. (3) The outside ambient pressure is standard (sea level) atmospheric pressure, and the ambient temperature is 20 °C. (4) The interfacial shear strength of the adhesive layer present between the exit cone and throat is 10MPa [32]; a bilinear cohesive zone model (CZM)[33] is used to simulate the interface state. (5) The metal flange edge is fixed. (6) The total simulation time is 21 seconds, which represents the typical duration of the test time of a solid rocket engine [32].

The calculations were performed on a Windows-based machine with a 4.8GHz CPU and 32GB RAM. The coupled-thermal displacement analysis method solver of ABAQUS-Standard TM (Version, 16.4-2) is used to directly couple the temperature and stress fields of the nozzle exit cone with the above loads and boundary conditions. In order to guarantee the accuracy of the initial temperature distribution, the same mesh density was used both for the thermal and structural models. The thermomechanical coupling element CAX4T (axisymmetric thermal

coupling quadrilateral linear element) was used, and the CAX3T (axisymmetric thermal coupled triangular linear element) was adopted to mesh the local region. An analysis of different mesh densities was performed to examine the dependency of the numerical results on the numbers of elements. After examining the stress distribution from different simulations it was found that the deviation of the maximum equivalent stress would not exceed 1% when the element size was less than 0.5×0.5mm. Hoever, local stress concentration regions usea finer mesh size. For all the other components, the elements side has a constant length of 1mm. The total number of elements in the multi-physics model is 7023, with 45 elements through the thickness.

2.2 Results of the numerical analysis

The overall structural temperature reaches its peak at the end of the time domain simulation. At the entrance of the throat the highest temperature is 3191 °C, and 2091 °C at the exit cone. The temperature of the external alloy steel is less than 30 °C at the end of the simulation.

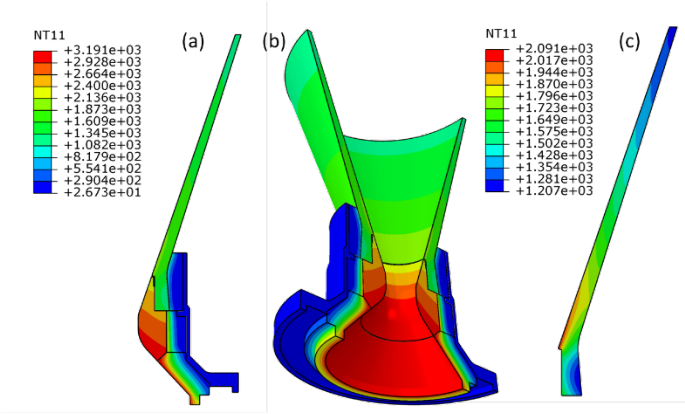

Fig. 3. Nozzle temperature contour of the final states: (a) two-dimensional cross-section, (b) a three-dimensional structure, (c) two-dimensional exit cone [Unit, °C]

The structural failure mode of the nozzle can be divided into material failure, and failure of the bonding between the different components. The material failure can be caused by the material ablation that induces erosion; another failure mode is represented by the local stress

that exceeds the strength of the material. Because this analysis is mainly concerned with the structural response of the system at the initial design stage iteration, effects like the mechanical and thermal erosion are neglected. The subsequent reliability analysis is therefore performed by only considering the failure mode represented by the structural stress exceeding the material strength.

2.2.1 Radial stress of the exit cone

The radial stress field of the exit cone is shown in Fig. 4(a). The maximum radial tensile stress occurs at point A, which is located at the sharp contact corner of the exit cone and the throat. During the thermal loading stress concentrations appear at this corner. The maximum radial tensile stress is 9.8MPa, which is significantly lower than the value of the material tensile strength (160MPa). While, the stress concentration at sharp corners does not represent the correct stress magnitude, it must be larger than the actual stress, so he radial tensile stress should not cause failure of the exit cone. The maximum radial compressive stress occurs at point B, with the compressive stress being mainly generated by the thermal expansion of the throat. The maximum radial compressive stress is 60.2MPa, which is again lower than the value of the material compressive strength (140MPa). The radial compressive stress therefore should not damage the exit cone.

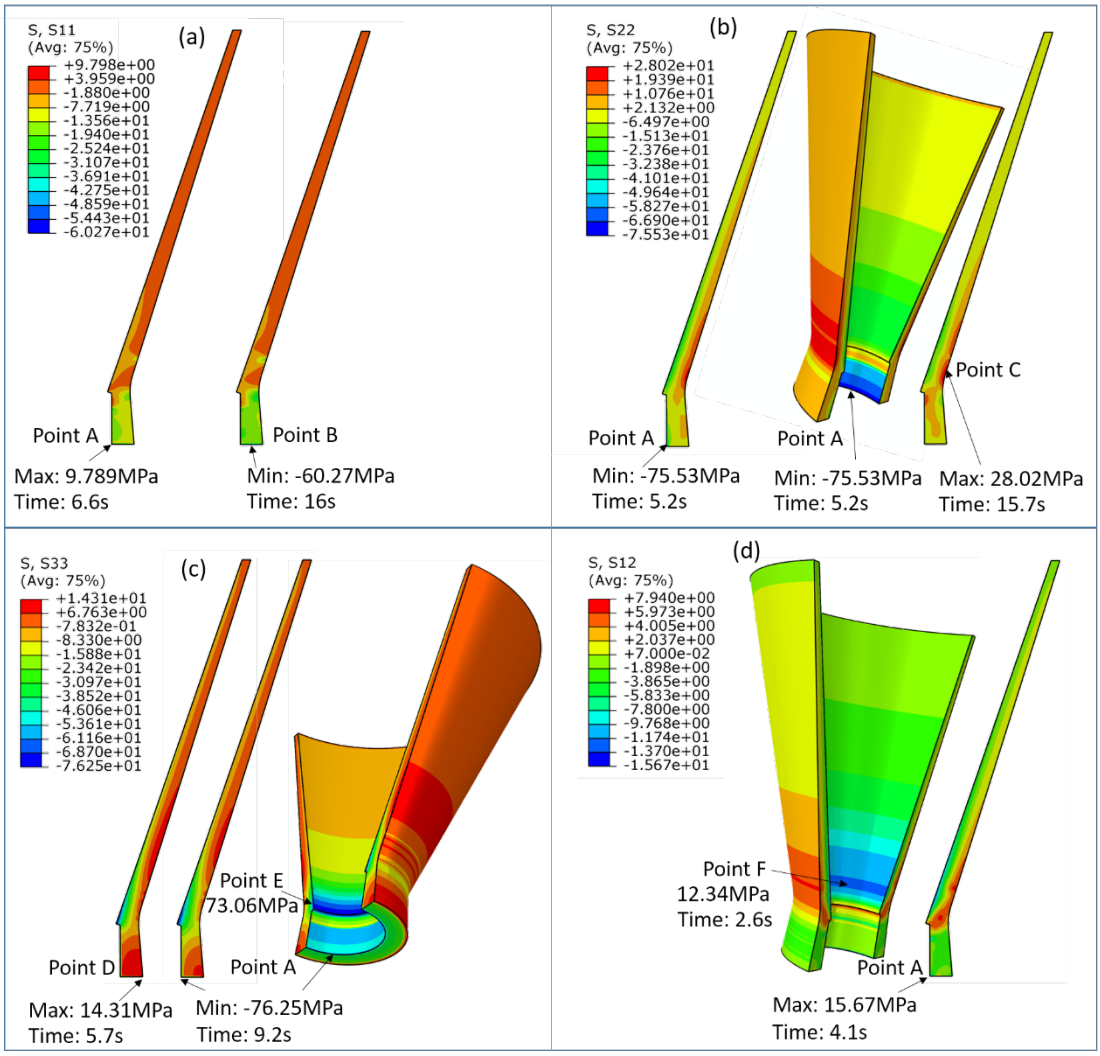

Fig. 4. The (a) radial, (b) axial, (c) hoop and (d) interlaminar shear stress contours of the exit cone

2.2.2 Axial stress at the exit cone

The axial stress field of the exit cone is shown in Fig. 4(b). The maximum axial tensile stress occurs at point C, which is located at the contact corner of the exit cone and the back wall. The maximum axial tensile stress is 28MPa, lower than the value of the material tensile strength. The maximum axial compressive stress is 75.5MPa after 5.2s. The maximum axial compressive stress occurs at point A. Because this particular location is close to the throat, it expands before the other adjacent surfaces. Compressive stresses are generated in this area because of the thermal expansion mismatch. Because the compressive strength of the material is 90MPa, if

one takes into account potential material uncertainties the axial compressive stress may be a source of failure for the nozzle.

The time histories of the stresses localized at points A, E, and F are shown in Fig. 5. The figure shows that the maximum axial compressive stress of the exit cone occurs after 5.2 seconds. At this time the adhesive layer between the exit cone and the throat is gradually degraded and therefore stress is released. The compressive stresses continue to decrease as time increases. After 11 seconds the adhesive layer is completely destroyed, and stress cannot be further released, with consequent leveling off.

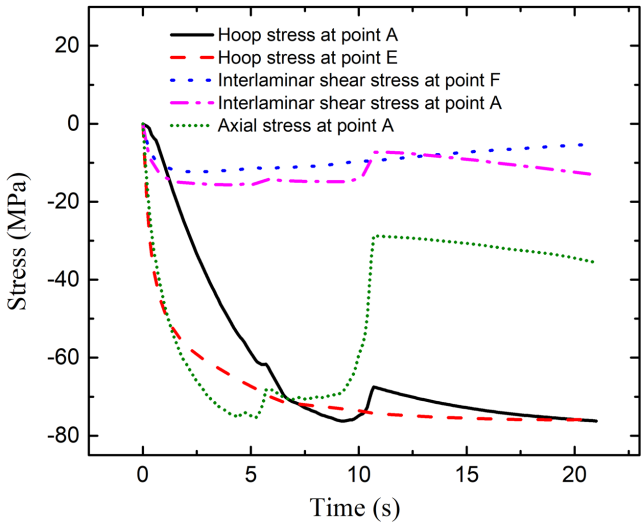

Fig. 5. Time histories of the stresses of the exit cone

2.2.3 Hoop stress of the exit cone

The distribution of the hoop stresses is shown in Fig. 4(c). The maximum hoop tensile stress occurs at point D located at the contact corner between the exit cone and the back wall. The maximum hoop tensile stress is 14.3MPa after 5.7s, again significantly lower than the material tensile strength. After 9.2s the hoop compressive stress reaches its maximum (76.2MPa) at point A. The hoop stress can also be observed in the annular region of the exit cone near point E. The maximum hoop compressive stress at point E is 75.93MPa at 19.2 sec. This position is

located in the front area of the exit cone, and it is exposed to the combustion flow. Although the temperature in this region is higher than in other areas, its hoop thermal expansion is constrained by the presence of the back wall and therefore a large compressive stress is generated. If uncertainty associated to the material properties is considered the hoop stresses at points A and E may exceed the compressive strength of the material (90MPa), and therefore cause failure of the exit cone.

From Fig. 5 it is possible to notice that between the time interval of 7s-10s the hoop compressive stress at point A is slightly higher than the stress at point E. During the remaining time the hoop stress at point E is always greater than the stress at point A. From the size of the pressure distribution area, the hoop stress at point A can only cause partial damage to the corner of the small area, and will not likely cause the failure of the whole structure. The hoop stress at point E may, however, induce failure.

2.2.4 Interlaminar shear stress of the exit cone

The interlaminar shear stress of the exit cone is shown in Fig. 4. (d). The figure shows that the maximum interlaminar shear stress occurs again at point A. The maximum interlaminar shear stress is 15.6MPa (at 4.1s). Another area of stress concentration is point F, with its maximum interlaminar shear stress at 12.3MPa. With the interlaminar shear strength equal to 26MPa, if material uncertainties are considered the interlaminar shear strength of point A and F may exceed the interlaminar shear strength of the material, and therefore cause failure of the exit cone. Delamination damage caused by shear failure may also occur in the circular area around point F.

In summary, the model identified three distinct modes that may lead to the failure of the exit cone: compressions along the axial and hoop directions, and interlaminar shear. The other failure modes are less likely to occur.

3 Reliability analysis of the exit cone

The structure of the nozzle is complex. The high combustion temperature and the internal gas flow velocity create an extremely harsh environment for the nozzle materials. Moreover, size scale effects given by the discrete nature of the C/C microstructure bring further uncertainties in determining the overall mechanical performance and directly affect the reliability of the nozzle structure.

3.1 Quantization of parameter uncertainty

In the probability model, the uncertainty comes from the discretization of the uncertainty from the variability of the material properties. The material properties are usually measured through experiments, and the uncertainty includes not only the natural dispersion of the properties, but also the testing errors. In this paper, the value of the structural strength at failure is also non-deterministic. For simplicity we assume that the material properties follow a normal distribution, and the strength has a uniform distribution. In order to facilitate the calculation, seven main material parameters are normalized as shown in Table 4, and the probability distribution types of material properties are also specified.

Table 4 uncertainty parameters and the distribution type of material

Parameter	Symbol	Distribution Type	Mean	Coefficient of Variation
Thermal expansion coefficient	*x1*	Normal Distribution	1.0	15%
Heat capacity	*x2*	Normal Distribution	1.0	30%
Radial thermal conductivity	*x3*	Normal Distribution	1.0	10%
Axial thermal conductivity	*x4*	Normal Distribution	1.0	3%
Axial elastic moduli	*x5*	Normal Distribution	1.0	10%
Radial elastic moduli	*x6*	Normal Distribution	1.0	10%
Density	*x7*	Normal Distribution	1.0	10%

Hoop compressive strength	*R3*	Uniform Distribution	140.0	10%
Axial compressive strength	*R2*	Uniform Distribution	90.0	5%
Shear strength	*R1*	Uniform Distribution	30.0	11.5%

3.2 Computational process

From the above analysis it is evident that there are three main factors leading to the failure of exit cone: axial compression, hoop compression and interlaminar shear failures. The maximum stress failure criterion is used to evaluate the reliability of the exit cone. Failure of the exit cone is assumed to occur if the stress is greater than the strength along specific directions. The maximum stress failure criterion does not consider interaction between the failure modes, but it is a conservative approximation of failure especially for combined tensile/shear/compressive loading.

Among the most common structural reliability analysis methods, response surfaces and Monte Carlo simulations are well developed and benchmarked. In this study we combine a surface response method (SRM) with finite elements, as well as Monte Carlo simulations to analyze the reliability. We first obtain the structural performance functions for the different failure modes by response surface approximation. To this end, 300 sample sets used to obtain the surface response are derived by optimization using Latin Hypercube sampling of the uncertainty space. Each set is computed independently by fitting higher order polynomials. We finally obtain a surface response for the three types of failure modes by higher order polynomial fit, and then the response surface is used for further reliability analysis (see the flowchart in Figure 6).

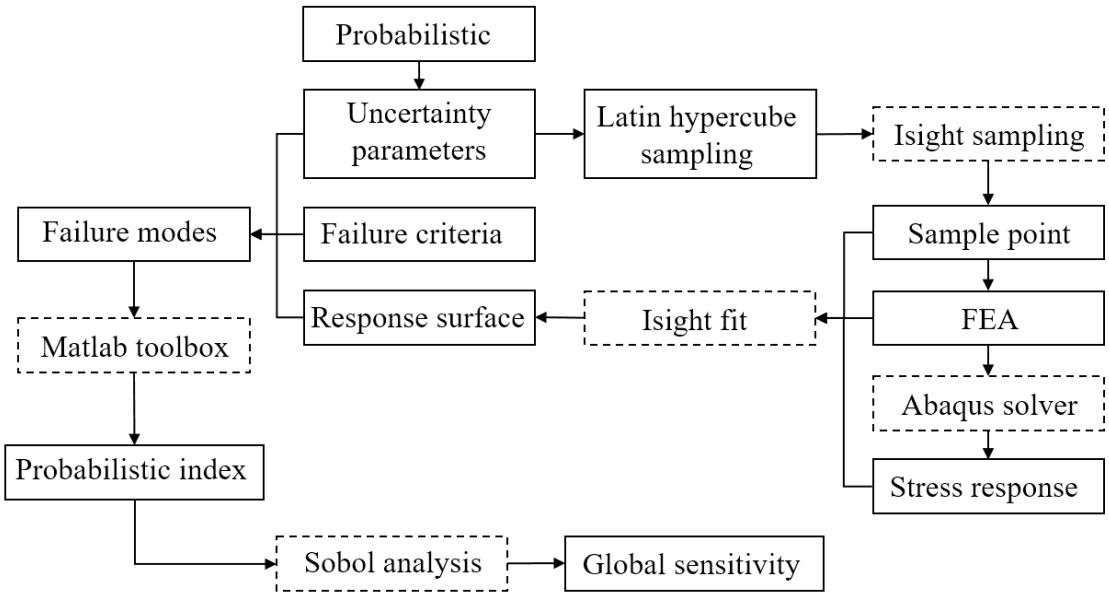

Fig. 6. Flowchart of computing process

3.3 Reliability analysis of the nozzle exit cone

3.3.1 Reliability based on probabilistic theory

The structural performance function of the exit cone can be represented by a two-dimensional function that relates response and capability. If R represents the capability – i.e. strength - and S is the response (stress), it is possible to denote the performance function as:

$$M = R - S \tag{3}$$

For the three failure modes concerned in this study the corresponding limit state functions can be presented as follows:

$$\begin{aligned} M_{12} &= R_1 - |S_{12}| \\ M_{22} &= R_2 - |S_{22}| \\ M_{33} &= R_3 - |S_{33}| \end{aligned} \tag{4}$$

Where R_1 and S_{12} are, respectively, the shear strength and shear stress; R_2 and S_{22} are the axial compressive strength and axial compressive stress; R_3 and S_{33} are the hoop compressive strength and stress, respectively. Using a classical SRM nonlinear quadratic regressive fit the expressions of the responses are:

$$S_{12} = -207 + 374x_6 - 8{x_4}^2 - 10{x_5}^2 - 223{x_6}^2 - 3.5{x_7}^2 - 6x_1x_3 - 10x_1x_5 + 16x_1x_6 - 6x_2x_3 + 5x_2x_4 - 9.7x_2x_5 + 10x_2x_6 + 2.7x_3x_4 + 5x_3x_5 + 7.3x_3x_7 + 8.3x_4x_6 + 36x_5x_6 \quad (5)$$

$$S_{22} = -59.8 - 6.4x_3 - 34x_4 + 7x_5 + 2{x_3}^2 + 14.4{x_4}^2 - 2.9{x_5}^2 + 1.7x_1x_2 + 0.9x_1x_4 + 2.8x_1x_5 - 5.4x_1x_6 - 1.6x_2x_3 - 20.7x_3x_4 + 9.4x_3x_5 + 8.8x_3x_6 \quad (6)$$

$$S_{33} = 16 - 15.8x_2 - 98.8x_3 - 38.6x_4 + 36.4x_5 - 21.6{x_3}^2 - 17.7{x_4}^2 - 19{x_5}^2 - 12.2{x_7}^2 - 3.6x_1x_4 - 13x_1x_5 + 16.9x_1x_7 + 16.4x_2x_3 + 43.8x_3x_4 - 21.6x_3x_6 + 20.2x_4x_5 + 16.3x_4x_6 + 6.4x_4x_7 \quad (7)$$

The subsequent reliability analyses from Monte Carlo simulations are performed based on these SRMs in order to reduce the computational expense. The reliability index β, failure probability P_f, and the standard deviation and coefficient of failure probability are calculated using a Monte Carlo method with 5,000 and 10,000 Monte Carlo simulations respectively (Table 5).

Table 5 Reliability of exit cone based on probability model

Stress	Sample	Reliability index, β	Failure Probability, P_f	Stdev(P_f)	CoV(P_f)
Interlaminar shear	N=5000	1.9357	0.0529	0.0032	5.98%
	N=10000	2.0480	0.0406	0.0020	4.86%
Axial compression	N=5000	1.5849	0.113	0.0045	3.98%
	N=10000	1.5853	0.1129	0.0032	2.8%
Hoop compression	N=5000	2.7944	0.0052	0.0010	19.56%
	N=10000	2.6921	0.0071	8.4E-4	11.83%

3.4 The results of the failure probability analysis

The reliability results for the three failure modes are listed in Table 6. The results show that the axial compression failure is the most likely cause of the structural failure. Failure can also occur by interlaminar shear, while hoop compression is the least likely of the three to cause failure.

Table 6 The failure probability of different conditions

Failure		
Interlaminar shear	Axial compression	Hoop compression
0.0406	0.1129	0.0071

3.5 Global sensitivity analysis

Variance based sensitivity analysis, namely Sobol analysis, is a form of global sensitivity analysis. It decomposes the variance of the output of the model or system into fractions which can be attributed to inputs or sets of inputs [34]. It would be very useful to identify the most significant input uncertain parameters that contribute to the variation of the different types of stress associated to these three failure modes. In this case study, the Sobol analysis method is used in this case to carry out the global sensitivity analysis [35]. The basis of the method consists in the decomposing the model output function into a sum of variance terms by using combinations of input parameters with increasing dimensionality. The variance decomposition can be expressed as:

$$V(output) = \sum_{i=1}^{n} V_i + \sum_{i \le j < n}^{n} V_{ij} + \cdots + \sum_{i \le n}^{n} V_{i \cdots n} \quad (8)$$

Where $V(output)$ is the total variance of the model output; V_i defined as the first order contribution of the ith model parameter; V_{ij} is the second order contribution of coupling effects of the ith and jth parameter; n means the number of model parameters. The importance of the given input factor is measured by a term defined as the sensitivity index, which is the fractional contribution to the output variance due to the uncertainties in the inputs. The Sobol sensitivity index can be expressed as:

$$S_I = V_i / V(output) \quad (9)$$

$$S_{IJ} = V_{ij} / V(output) \quad (10)$$

$$S_{Ti} = 1 - V_{\sim i} / V(output) \quad (11)$$

S_I is the first order Sobol sensitivity index, S_{IJ} denotes as the second order term and S_{Ti} denotes as the total Sobol sensitivity index corresponding to the ith model parameter. The resulting Sobol's sensitivity indices therefore rely on not only the input parameter distribution,

but also the contribution of the input parameter in the mathematical model. The first order Sobol indices S_I are used to quantify the separate effect on the failure modes of each input parameter, while the total Sobol indices S_{Ti} quantify the total effect of the input parameter, which include both the first order effect and also its interactions with the other input variables [36].

The use of Polynomial Chaos Expansion (PCE) techniques is widely recognized as a quick way to directly compute the Sobol sensitivity indices. PCE is therefore employed in this case study. Since the distribution of the input parameters (i.e., the thermal expansion coefficient, heat capacity, radial thermal conductivity, axial thermal conductivity, axial elastic moduli, radial elastic moduli and density) are assumed to have normal distributions, the PCE surface response is generated based on the Gaussian probabilistic distribution by using Hermite orthogonal polynomials. A linear enumeration strategy is employed to construct the multivariate orthonormal basis. The multivariate orthonormal basis is then truncated by using a fixed strategy to build the complete basis with respect to a maximal degree of four [37]. A non-intrusive method based on least squares minimization is used to optimize the PCE coefficients using 200 sampling points generated by the FE model. With this PCE response surface model, the Sobol's indices can then be computed directly without further Monte Carlo simulations.

Figure 7 shows the first order and total Sobol's indices of these seven uncertain parameters for the three failure modes separately. The result shows that the indices of these uncertain parameters share very similar trends related to the axial compressive failure (Figure 7 (a)), hoop compression failure (Figure 7 (b)) and shear failure (Figure 7 (c)). Both types of indices clearly show that the axial thermal conductivity has the highest impact on the variation of the outputs (First order: 28%, 36% and 36%; Total: 60%, 70% and 70%), despite the coefficient of variation

(CoV) of its uncertain distribution shown in Table 4 is the smallest among the seven input variables. The radial thermal conductivity comes second in terms of impact. However, in terms of total contributions, the second largest influence comes from the elastic moduli for the axial compression failure (25%). For the hoop compression and shear failures, the radial elastic moduli and the density equally take the second leading contributions by about 21%. This suggests that the coupling contribution from the elastic moduli and density is more significant than the one from the thermal conductivity and the elastic moduli along the radial direction. The first order Sobol's indices clearly show that the thermal expansion coefficient and heat capacity provide negligible contributions to all the three failure modes. These two parameters could be therefore excluded in future uncertainty analysis.

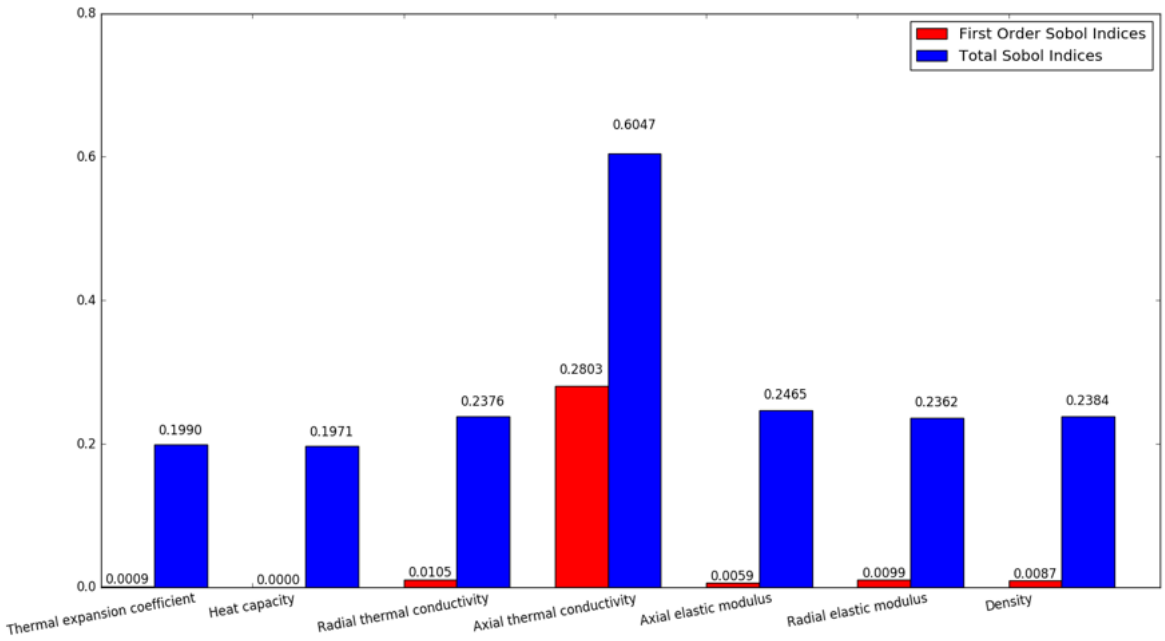

(a)

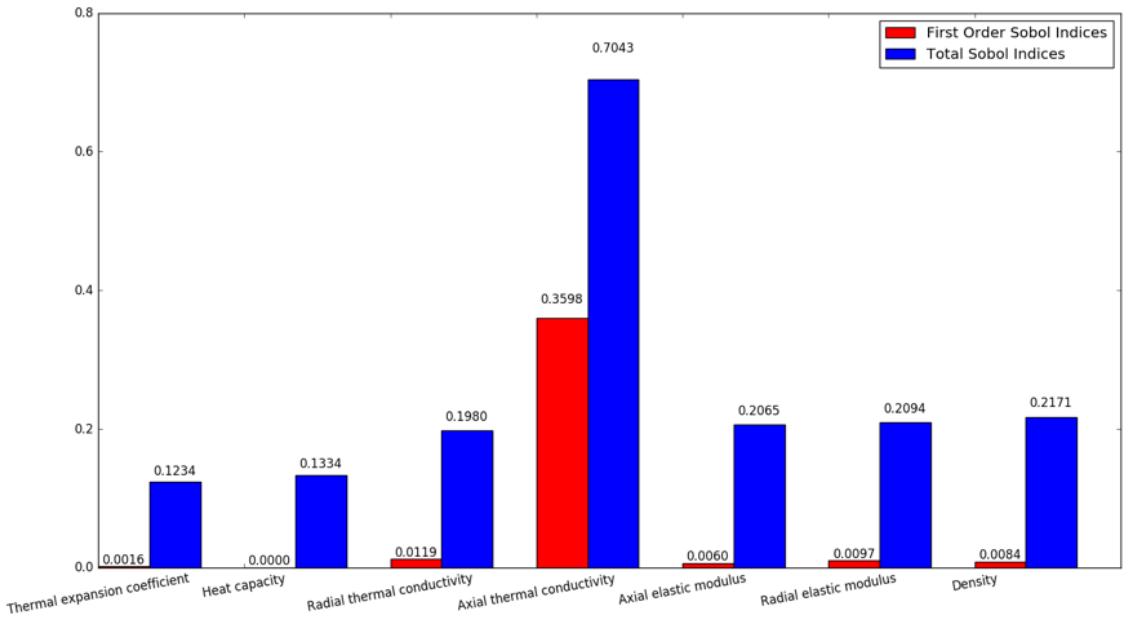

(b)

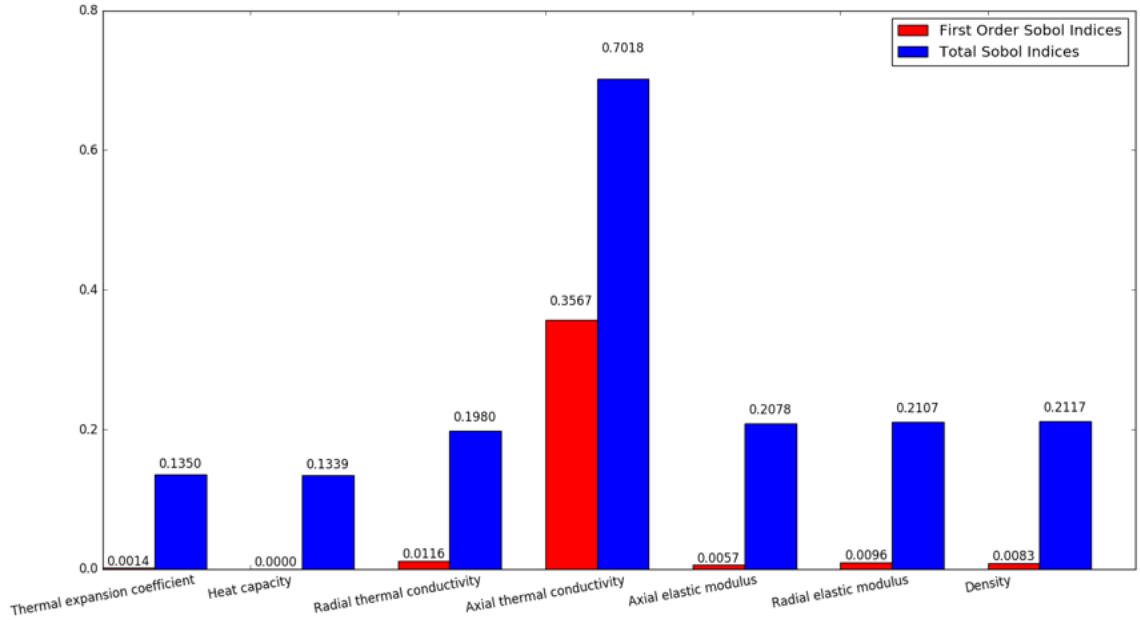

(c)

Figure 7 Sobol's indices ranking of the input uncertain variables according to their influence on: (a) the axial compressive failure (b) the hoop compression failure and (c) shear failure

4 Conclusions

In this paper we have used a probabilistic model to account for uncertainties in the material properties of a solid rocket nozzle exit cone made from carbon/carbon composites, adhesive layers and metal components and simulate the structural response. To this end we combine a finite element model and a surface response method to compute the structural reliability by considering three types of failure modes. The methodology here has been developed to provide a way to calculate the reliability of nozzle-type structures in the case of small sample data populations. A sequentially coupled thermal/structural analysis shows that under the service environment conditions reproduced in this study the axial compressive, hoop compressive and interlaminar shear stresses are close to the material strength, while the stress along other directions is relatively small. If we ignore local stress concentration in the corners of the exit cone, the most likely failure region is in the contact area between the exit cone and the throat induced by the axial compressive stress. Also, another critical area is represented by the front region of the exit cone exposed to the combustion chamber, which is characterized by the presence of hoop compressive stresses. The third possible failure mode is the interlaminar shear failure, which is located at the region of the exit cone far away to the throat.

A global sensitivity analysis also was carried out to identify the most influential input parameters on these three failure modes. A Sobol analysis was used to rank the impacts of the input parameters based on the PCE response surface model. The results show that the axial thermal conductivity has the highest contribution on all the three modes. The contributions from the thermal expansion coefficient and heat capacity are negligible. The conclusions from this probabilistic analysis are quite useful to streamline and optimize the outcome of the initial design stage for these C/C composite nozzles. The importance of the axial thermal conductivity

in this type of structure may lead to a design of C/C composites and their stacking sequences that favor a strong unidirectional thermal conductivity response for the nozzle configuration. In a similar manner, the design and materials selection of these types of nozzles can be streamlined to prevent the axial compression failure, which is the most important failure mode of the system. Compressive failure in C/C composites can be tailored by fibers architectures or needle-punch techniques[38], and these approaches could be used to increase the reliability of these carbon-based nozzle designs.

Acknowledgements

This research is sponsored by the National Natural Science Foundation of China (11672088) and the National Basic Research Program of China (No. 2015CB655200). The authors are also grateful for the financial support from National key Laboratory of Science and Technology on Reliability and Environmental Engineering.

Reference

1. Li, K.-Z., Shen, X.-T., Li, H.-J., Zhang, S.-Y., Feng, T., and Zhang, L.-L. "Ablation of the carbon/carbon composite nozzle-throats in a small solid rocket motor," *Carbon* Vol. 49, No. 4, 2011, pp. 1208-1215.
2. Peng, L.-n., He, G.-q., Li, J., Wang, L., and Qin, F. "Effect of combustion gas mass flow rate on carbon/carbon composite nozzle ablation in a solid rocket motor," *Carbon* Vol. 50, No. 4, 2012, pp. 1554-1562.
3. Liu, Y., Pei, J.-q., Li, J., and He, G.-q. "Ablation characteristics of a 4D carbon/carbon composite under a high flux of combustion products with a high content of particulate alumina in a solid rocket motor," *New Carbon Materials* Vol. 32, No. 2, 2017, pp. 143-150.
4. Zaman, W., Li, K.-z., Ikram, S., and Li, W. "Residual compressive and thermophysical properties of 4D carbon/carbon composites after repeated ablation under oxyacetylene flame of 3000 °C," *Transactions of Nonferrous Metals Society of China* Vol. 23, 2013, pp. 1661-1667.
5. Vignoles, G., Aspa, Y., and Quintard, M. "Modelling of carbon–carbon composite ablation in rocket nozzles," *Composites Science and Technology* Vol. 70, No. 9, 2010, pp. 1303-1311.
6. Sciti, D., Zoli, L., Silvestroni, L., Cecere, A., Martino, G. D. D., and Savino, R. "Design, fabrication and high velocity oxy-fuel torch tests of a C f -ZrB 2 - fiber nozzle to evaluate its potential in rocket motors," *Materials & Design* Vol. 109, 2016, pp. 709-717.
7. Shen, X.-T., Liu, L., Li, W., and Li, K.-Z. "Ablation behaviour of C/C–ZrC composites in a solid rocket

motor environment," *Ceramics International* Vol. 41, No. Part B, 2015, pp. 11793-11803.

8. Cai, T., and Hou, X. "A simple method for tackling moving boundary in numerical simulation of temperature response of the solid rocket motor," *26th AIAA Aerospace Sciences Meeting*. Vol. 1, 1988.
9. Davis, D. W., and Phelps, L. H. "Thermal analysis of the MC-1 chamber/nozzle," 2001.
10. Wang, Y.-j., Li, J., Qin, F., He, G.-q., and Shi, L. "Study of thermal throat of RBCC combustor based on one-dimensional analysis," *Acta Astronautica* Vol. 117, 2015, pp. 130-141.
11. Heller, R. A., Yeo, I., and Thangjitham, S. "A Probabilistic Method to Establish the Reliability of Carbon-Carbon Rocket Motor Nozzles. Volume 2. Reliability and Failure Analyses of 2-D Carbon-Carbon Structural Components." United States, North America, 1992.
12. Heller, R. A., Thangjitham, S., and Wang, X. "A Probabilistic Method to Establish the Reliability of Carbon-Carbon Rocket Motor Nozzles. Volume 3. Stress and Reliability Analysis of Layered Composite Cylinders Under Thermal Shock." United States, North America, 1992.
13. Morozov, E., and de la Beaujardiere, J. P. "Numerical simulation of the dynamic thermostructural response of a composite rocket nozzle throat," *Composite Structures* Vol. 91, No. 4, 2009, pp. 412-420.
14. de la Beaujardiere, J.-F. P., Morozov, E. V., and Bright, G. "Numerical Simulation of the Aerothermostructural Response of a Composite Solid Rocket Nozzle During Motor Ignition." 45th AIAA/ASME/SAE/ASEE Joint Propulsion Conference & Exhibit, 2-5 August, 2009. AIAA 2009-4891, 2009.
15. Kumar, R. R., Vinod, G., Renjith, S., Rajeev, G., Jana, M., and Harikrishnan, R. "Thermo-structural analysis of composite structures," *Materials Science and Engineering: A* Vol. 412, No. 1, 2005, pp. 66-70.
16. Goyal, V., Rome, J., and Schubel, P. "Structural Analysis of Solid Rocket Motors," *Aiaa/asme/asce/ahs/asc Structures, Structural Dynamics, and Materials Conference Aiaa/asme/ahs Adaptive Structures Conference 10t*. 2013.
17. Turchi, A., Bianchi, D., Nasuti, F., and Onofri, M. "A numerical approach for the study of the gas–surface interaction in carbon–phenolic solid rocket nozzles," *Aerospace Science and Technology* Vol. 27, No. 1, 2013, pp. 25-31.
18. Bozkaya, K., Kuran, B., Hasanoglu, M., Yildirim, M., and Ak, M. "Effects of Production Variations on the Reliability of a Solid Rocket Motor," *Aiaa/asme/sae/asee Joint Propulsion Conference & Exhibit*. 2013.
19. Bozkaya, K., Sumer, B., Kuran, B., and Ak, M. A. "Reliability analysis of a solid rocket motor based on response surface method and Monte Carlo simulation," *AIAA* Vol. 3598, 2005, p. 2005.
20. Akpan, U., and Wong, F. "The Role of Probabilistic Sensitivity Analysis in Assessing the Service Life of Solid Rocket Motors," *Aiaa/asme/asce/ahs/asc Structures, Structural Dynamics, and Materials Conference*. 2006.
21. Kim, D.-S., Yoo, J., Park, S. H., Choi, J.-H., and Deogyang-gu, G.-s. "Reliability prediction of solid rocket considering uncertainties of failure mode," *3rd International Conference on Materials andReliability*. 2015.
22. Tu, C. V., and Wood, D. H. "Wall pressure and shear stress measurements beneath an impinging jet," *Experimental Thermal and Fluid Science* Vol. 13, No. 4, 1996, pp. 364-373.
23. Dombrovsky, L. A. "Radiation heat transfer in a supersonic nozzle of a solid-propellant rocket engine," *Thermopedia*. 2011.

24. Back, L. H., Massier, P. F., and Gier, H. L. "Convective heat transfer in a convergent-divergent nozzle," *International Journal of Heat and Mass Transfer* Vol. 7, No. 5, 1964, pp. 549-568.
25. Ahmad, R. A. "Convective Heat Transfer in the Reusable Solid Rocket Motor of the Space Transportation System," *Heat Transfer Engineering* Vol. 26, No. 10, 2005, pp. 30-45.
26. Pearce, B. E. "Radiative heat transfer within a solid-propellant rocket motor," *Journal of Spacecraft and Rockets* Vol. 15, No. 2, 1978, pp. 125-128.
27. Sun, L., Bao, F., Zhao, Y., Hou, L., Hui, W., Zhang, N., and Shi, W. "Crack cause analysis of a graphite nozzle throat insert," *Acta Astronautica* Vol. 137, No. Supplement C, 2017, pp. 70-77.
28. Sun, L., Bao, F., Zhang, N., Hui, W., Wang, S., Zhang, N., and Deng, H. "Thermo-Structural Response Caused by Structure Gap and Gap Design for Solid Rocket Motor Nozzles," *Energies* Vol. 9, No. 6, 2016, p. 430.
29. Ren, J., Li, K., Zhang, S., and Yao, X. "Dynamic fatigue of two-dimensional carbon/carbon composites," *Materials Science & Engineering A Structural Materials Properties Microstructure & Processing* Vol. 570, No. 7, 2013, pp. 123-126.
30. Thakre, P., and Yang, V. "Chemical Erosion of Refractory-Metal Nozzle Inserts in Solid-Propellant Rocket Motors," *Journal of Propulsion & Power* Vol. 25, No. 25, 2012, pp. 40-50.
31. Kou, G., Guo, L. J., and Li, H. J. "Effect of copper on the heat erosion mechanism of carbon/carbon composites," *Journal of Alloys & Compounds*, 2017.
32. Peng, T. "Reliability research and sensitivity analysis for carbon/carbon exit cone's material parameters," *Mechanics of Engineering*. Vol. Master, Harbin Institute of Technology, Harbin, 2015, p. 83.
33. Hibbitt, D. K., B.; Sorensen, P. *ABAQUS Standard User's and Reference Manuals (Version 6.14)*. USA: Johnston, RI, 2014.
34. Prieur, C., and Tarantola, S. "Variance-Based Sensitivity Analysis: Theory and Estimation Algorithms." 2017, pp. 1217-1239.
35. Wan, H., Xia, J., Zhang, L., She, D., Xiao, Y., and Zou, L. *Sensitivity and Interaction Analysis Based on Sobol' Method and Its Application in a Distributed Flood Forecasting Model*, 2015.
36. Saltelli, A., Annoni, P., Azzini, I., Campolongo, F., Ratto, M., and Tarantola, S. "Variance based sensitivity analysis of model output. Design and estimator for the total sensitivity index," *Computer Physics Communications* Vol. 181, No. 2, 2010, pp. 259-270 %@ 0010-4655.
37. Gratiet, L. L., Marelli, S., and Sudret, B. "Metamodel-based sensitivity analysis: polynomial chaos expansions and Gaussian processes," *Handbook of Uncertainty Quantification*, 2016, pp. 1-37 %@ 3319112597.
38. Li, D.-s., Luo, G., Yao, Q.-q., Jiang, N., and Jiang, L. "High temperature compression properties and failure mechanism of 3D needle-punched carbon/carbon composites," *Materials Science and Engineering: A* Vol. 621, 2015, pp. 105-110.